HHS Public Access

Author manuscript

Cancer Immunol Res. Author manuscript; available in PMC 2018 November 04.

Published in final edited form as:

Cancer Immunol Res. 2018 April ; 6(4): 422–433. doi:10.1158/2326-6066.CIR-17-0263.

TNFα and Radioresistant Stromal Cells Are Essential for Therapeutic Efficacy of Cyclic Dinucleotide STING Agonists in Nonimmunogenic Tumors

Brian J. Francica[1,2], **Ali Ghasemzadeh**[2,3], **Anthony L. Desbien**[1], **Debebe Theodros**[2], **Kelsey E. Sivick**[1], **Gabrielle L. Reiner**[1], **Laura Hix Glickman**[1], **Ariel E. Marciscano**[2], **Andrew B. Sharabi**[2,4], **Meredith L. Leong**[1], **Sarah M. McWhirter**[1], **Thomas W. Dubensky Jr**[1], **Drew M. Pardoll**[2], and **Charles G. Drake**[2,3]

[1]Aduro Biotech, Berkeley, California [2]Bloomberg-Kimmel Institute for Cancer Immunotherapy, Johns Hopkins University School of Medicine, Baltimore, Maryland [3]Department of Medicine, Division of Hematology/Oncology, Herbert Irving Comprehensive Cancer Center, Columbia University Medical Center, New York, New York [4]University of California San Diego School of Medicine, San Diego, California

Abstract

The cGAS-STING cytosolic DNA sensing pathway may play an integral role in the initiation of antitumor immune responses. Studies evaluating the immunogenicity of various cyclic dinucleotide (CDN) STING agonists administered by intratumoral (i.t.) injection showed potent induction of inflammation, tumor necrosis, and, in some cases, durable tumor-specific adaptive immunity. However, the specific immune mechanisms underlying these responses remain incompletely defined. The majority of these studies have focused on the effect of CDNs on immune cells but have not conclusively interrogated the role of stromal cells in the acute rejection of the CDN-injected tumor. Here, we revealed a mechanism of STING agonist-mediated tumor

Corresponding Author: Charles G. Drake, Columbia University, 177 Fort Washington Avenue, Suite 6GN-435, New York, NY 10032. Phone: 646-317-5290; Fax: 212-305-3035; cgd2139@cumc.columbia.edu.

Authors' Contributions

Conception and design: B.J. Francica, A. Ghasemzadeh, A.E. Marciscano, A.B. Sharabi, T.W. Dubensky Jr, D.M. Pardoll, C.G. Drake

Development of methodology: B.J. Francica, A.L. Desbien, A.E. Marciscano, A.B. Sharabi

Acquisition of data (provided animals, acquired and managed patients, provided facilities, etc.): B.J. Francica, A. Ghasemzadeh, A.L. Desbien, D. Theodros, K.E. Sivick, G.L. Reiner, L.H. Glickman, A.E. Marciscano

Analysis and interpretation of data (e.g., statistical analysis, biostatistics, computational analysis): B.J. Francica, A.L. Desbien, G.L. Reiner, L.H. Glickman, A.E. Marciscano, D.M. Pardoll, C.G. Drake

Writing, review, and/or revision of the manuscript: B.J. Francica, A. Ghasemzadeh, A.L. Desbien, D. Theodros, K.E. Sivick, L.H. Glickman, A.E. Marciscano, A.B. Sharabi, M.L. Leong, S.M. McWhirter, T.W. Dubensky Jr, C.G. Drake

Administrative, technical, or material support (i.e., reporting or organizing data, constructing databases): B.J. Francica, A.L. Desbien, A.E. Marciscano

Disclosure of Potential Conflicts of Interest

A.L. Desbien is a scientist at Aduro Biotech and reports receiving a commercial research grant from the same. K.E. Sivick has ownership interest in a patent with Aduro Biotech. C.G. Drake reports receiving a commercial research grant from Aduro Biotech. No potential conflicts of interest were disclosed by the other authors.

Note: Supplementary data for this article are available at Cancer Immunology Research Online (http://cancerimmunolres.aacrjournals.org/).

response that relied on both stromal and immune cells to achieve tumor regression and clearance. Using knockout and bone marrow chimeric mice, we showed that although bone marrow–derived TNFα was necessary for CDN-induced necrosis, STING signaling in radioresistant stromal cells was also essential for CDN-mediated tumor rejection. These results provide evidence for crosstalk between stromal and hematopoietic cells during CDN-mediated tumor collapse after i.t. administration. These mechanistic insights may prove critical in the clinical development of STING agonists.

Background

The immune system evolved to recognize, interpret, and combat infection using a series of diverse receptors that recognize evolutionarily conserved viral and bacterial molecules termed pathogen-associated molecular patterns (PAMP). The receptors, termed pattern recognition receptors (PRR), are expressed on a variety of immune and nonimmune cells and are essential for first sensing, then initiating, innate immune responses against a variety of pathogens (1–3). Downstream of PAMP–PRR ligation are a variety of transcription factors, including IRF-3 and NF-κB, that lead to the transcription of innate effector molecules, including IFNβ, TNFα, IFNγ, and IL1 (4). These effector cytokines execute a variety of antimicrobial effects, ranging from activation to apoptosis in both stromal and immune cells.

One such PAMP is cytosolic double-stranded (ds)DNA, which binds to cyclic GMP-AMP (cGAMP) synthase (cGAS). Upon dsDNA binding, cGAS catalyzes the conversion of ATP and GTP into cGAMP (5–7). In turn, cGAMP binds to stimulator of interferon genes (STING), an endoplasmic reticulum-resident protein initially discovered as an essential gene for expression of IFNβ by host cells infected with herpes simplex virus (HSV-1; refs. 8–10). In response to binding cGAMP or other cyclic dinucleotide (CDN) structures, STING phosphorylates the adaptor protein TBK1, which, in turn, phosphorylates IRF-3 and initiates the transcription of a number of interferon-stimulated genes, including type I interferons (9, 11–13) and other coregulated host defense pathways, including the NF-κB and STAT6 pathways (14, 15).

The cGAS-STING pathway initiates innate immune responses to multiple viral and bacterial pathogens. CDNs are expressed ubiquitously by bacteria to signal between microbes and regulate diverse metabolic processes. For example, the intracellular bacterium *Listeria monocytogenes* (Lm) produces cyclic-di-adenosine monophosphate (AMP), which, when secreted intracellularly through multidrug efflux pumps, binds and activates STING and results in the expression of IFNβ and other coregulated genes (16, 17). However, in mice, enhanced activation of STING suppresses the magnitude of Lm-induced $CD8^+$ T-cell priming specific for encoded antigens and diminishes protection against lethal wild-type (WT) Lm challenge, and conversely, mice lacking functional STING are more resistant to infection with intracellular bacteria, including Lm (18). The cGAS–STING signaling axis is also activated by dsDNA viruses, including pox viruses, adenoviruses, gamma herpes viruses such as HSV, and retroviruses such as HIV and HTLV (5, 15, 19–24). In response to infection with dsDNA viruses, induced cGAMP can be transported to neighboring cells

through gap junctions and inhibit virus spread, supporting the central role of this pathway as a major antimicrobial defense mechanism (25, 26). However, the mechanisms underlying the observation that cGAS—STING-deficient mice are more sensitive to virus infection but are more resistant to infection with intracellular bacterium are not yet understood.

Results from several laboratories suggest that the cGAS-STING pathway may have evolved to recognize host cell damage by sensing of “self” DNA. STING-deficient mice have a significantly reduced ability to reject immunogenic tumors, and poorly immunogenic tumors have accelerated growth in these mice as compared with WT mice (27). Tumor DNA can be detected in cross-presenting $CD8\alpha^+$ DCs, and depletion of this antigen-presenting cell population results in both the significant decrease of IFNβ expression and reduced antitumor immunity (27). These studies suggest that the cGAS–STING is a critical pathway for sensing host cell damage. Sparked by these discoveries, preclinical and clinical studies are testing CDNs as an antitumor immunotherapeutic agent administered either systemically [intravenous (i.v.)] or locally [intratumoral (i.t.); refs. 27–35]. Clinical activity seen with i.t. injection of a modified HSV-1 vector encoding GM-CSF (talimogene laherparepvec, or T-VEC), provides evidence that the STING pathway may regulate tumor immunity in humans and supports the rationale for targeting STING directly with CDNs.

Although previous investigations showed that local or systemic activation of STING results in significant and durable antitumor immunity, the critical innate and adaptive immunologic mechanisms underlying these responses are not completely understood. In part, it is difficult to draw unifying conclusions due to the different CDN structures, dose levels, and treatment regimens used in previous investigations. For example, administration of low doses of CDN i.v. can prime a systemic tumor-specific immune response, but antitumor immunity can be suppressed at high CDN dose levels (33). In contrast, i.t. administration of doses of 25 to 200 μg of certain CDNs can induce local antitumor efficacy, systemic antitumor immunity, and immunological memory (31, 35).

Several CDN molecular structures have been evaluated in mice. The natural product of cGAS is 2′–5′, 3′–5′ cGMP-AMP (2′3′ cGAMP), and CDNs with this internucleotide bridge structure are collectively referred to as “mixed linkage” or “noncanonical linkage” CDNs and have about a 10-fold increased STING-binding affinity. CDNs with a noncanonical 2′3′ structure are more potent activators of human STING than the canonical bis 3′-5′ CDNs produced by bacteria (35). The notion that STING can distinguish between bacterial and host cGAS—produced ligands and is activated more profoundly by host-produced 2′3′ cGAMP is suggestive that the cGAS-STING pathway evolved principally to sense host damage and dsDNA-based pathogens rather than bacterial produced CDNs. Nevertheless, this dichotomy between metazoan and bacterial CDN structures provided important insights into the development of synthetic CDN compounds for evaluation in humans. In this investigation, we utilized a synthetic CDN known as ADU-S100 that is being evaluated in patients with advanced cancers that are resistant to standard-of-care therapies. The structure of ADU-S100 has been described previously (31, 35) and is disodium dithio-(R_P, R_P)-[cyclic [A(2′,5′)pA(3′,5′)p]], a cyclic di-ribonucleotide composed of two AMP analogues cyclized via a 2′,5′ (noncanonical) and a 3′,5′ (canonical) phosphodiester bond. ADU-S100 has been shown to bind and activate all five

human STING polymorphic proteins. Other formulations of CDN and STING agonists have been used preclinically, administered in a variety of vaccination settings, and have shown a range of efficacies in tumor clearance, induction of cytokines, and activation of an adaptive immune response.

Here, we found that TNFα is definitively required for CDN-mediated acute tumor necrosis and modulation of the immune infiltrate. Through the use of bone marrow chimeras, we provide evidence that stromal cells also respond to STING agonists and, thus, play a critical role in mediating acute clearance of tumors during i.t. CDN therapy. Collectively, our results outline a model in which both stromal and hematopoietic cells are involved in the CDN-mediated antitumor immune responses.

Materials and Methods

Cell lines and mice

B16F10, CT26, MC38, and 4T1 mouse cell lines were acquired from ATCC and were cultured in complete RPMI consisting of 10% FBS, penicillin (100 U/mL), streptomycin (100 μg/mL), 1 mmol/L sodium pyruvate, and NEAA. BT549, H460, T47D, MALME-3M, MCF7, SK-MEL-28, SK-MEL-5, SK-MEL-2, and THP-1 human cell lines were acquired from ATCC and cultured as recommended by ATCC. B16F10, MC38, 4T1, and CT26 cells were validated as *Mycoplasma* negative using the STAT-Myco test by IDEXX Incorporated. Cells were thawed from liquid nitrogen stocks and passaged 2 to 3 times before being used for *in vivo* or *in vitro* experimentation.

Six- to 8-week-old female C57BL/6 and BALBc mice were purchased from The Jackson Laboratory or Charles River, and 6–8-week-old female BL6-CD45.1 mice were purchased from Charles River. cGAS$^{-/-}$ animals were a generous gift from Dr. Skip Virgin at the University of Washington, St. Louis. STING$^{-/-}$ mice were the Golden Ticket strain (C57BL/6J-*Tmem173*^{gt}/J) and were a gift from Dr. Young Kim. Rag2$^{-/-}$ animals were a gift from Dr. Jonathan Powell. IFNα$^{-/-}$ (B6.129S2-Ifnar1tm1 Agt/Mmjax), TNFα$^{-/-}$ (B6.129S-Tnftm1Gkl/J), and IL6$^{-/-}$ (B6.129S2-Il6tm1Kopf/J) breeder pairs were purchased from The Jackson Laboratories and bred in Johns Hopkins Facilities. All mouse procedures were approved by the Johns Hopkins University or Aduro Biotech Institutional Animal Care and Use Committee under protocol number M013M08 and were compliant with the Guide for the Care and Use of Laboratory Animals (8th ed., The National Academic Press, 2011).

Chimeric animals were generated by irradiating 6–12-week-old CD45.1, TNFα$^{-/-}$, and Golden Ticket mice with two doses of 6 gy separated by 3 hours. Three hours after the second dose of irradiation, mice were reconstituted with 5 to 10 million cells of nonirradiated donor bone marrow via tail vein injection, and left to rest for at least 6 weeks. To confirm reconstitution, mice were bled 5 to 6 weeks after irradiation, and PBMCs were stained for CD45.1 (WT) and CD45.2 (Golden Ticket). All chimeric animals were put on uniprim feed at least 1 week before irradiation and removed from uniprim feed at least 1 week before tumor challenge.

Tumor outgrowth and infiltration studies

A total of 5×10^5 B16F10 cells were implanted between the skin and peritoneal cavity on day 0. Tumors were monitored until the group average was about 80 mm^3 and then treated with 100 μg i.t. injections of CDN in 40 μL PBS or with PBS alone every other day for a total of three treatments. For chimera studies, mice were implanted with tumor cells, and when tumors were palpable, animals were selected and arranged in groups normalized to about 80 mm^3. In TNFα blockade experiments, the clinical reagent Enbrel (Amgen) or human IgG1 isotype control (Cat# BE0297; Bio X Cell) was administered intraperitoneally at 1 mg/mL in 200 μL. Tumor outgrowth volume was measured with calipers, and volume was calculated using the equation $V = {}^1/_2$ (width^2 × length). Animals were sacrificed when tumor volumes exceeded 2,000 mm^3.

Flow cytometry

Tumors and tumor-draining inguinal lymph nodes (TDLNs) were excised from animals sacrificed 24 hours after i.t. CDN injection in media containing 10% FBS, penicillin (100 U/mL), and streptomycin (100 μg/mL). These tissues were manually dissociated with scissors and syringe plungers, filtered with 70-μm mesh, manually dissociated over a 70-μm mesh filter a second time if needed, then resuspended for antibody staining. Flow cytometry antibodies included: from BioLegend— CD11b-AF700 (M1/70), CD11c-FITC (N418), CD86-PE (GL-1), CD19-PerCP-Cy5.5 (6D5), Ly6C-BV605 (HK1.4), CD45.2-APC (104), IA/IE-PerCP-Cy5.5 (M5/114.15.2), Ly6G-BV421 (1A8), CD16/32-BV510 (93), F4/80-PE-Cy7 (BM8), Ly6c–PerCP-Cy5.5 (HK1.4), and CD4-BV605 (GK1.5) from EBioscience— NK1.1-PE (PK136) and CD8–PE-Cy7 (53-6.7); CD4-Pacific Orange (RM4-5) from Life Technologies; and CD45.1-FITC (A20) from BD Pharmingen. Samples were analyzed using an LSR II cytometer with FACSDiva software (BD Biosciences), and data were quantified using FlowJo software (Tree Star, Inc.) or Cytobank (Cytobank, Inc.).

Cytokine analyses

Tumor cytokines were quantified by either luminex or by ELISA. Luminex analysis was performed using the Cytokine and Chemokine 36-Plex Mouse ProcartaPlex Panel 1a (Cat# EPX360-26092-901) array. Tumors were collected in 1 mL PBS and disrupted with manual and GentleMacs (Miltenyi Biotec) dissociation. TDLNs were collected similarly in 1 mL PBS and dissociated with syringe plungers and then spun to remove cellular matter. Lysates for luminex analysis were taken directly from the 1 mL solution and plated according to the manufacturer's suggestions. To reduce luminex sample volume, the DropArray LT210 Washing Station MX (Cat# LT-210MX-01-01; Curiox) was used with microbead plates (Curiox, Cat# 96-CC-BD-05). These plates were then run on using the Bio-Plex 200 (Bio-Rad, Cat#171-000201).

Material for ELISAs was prepared by resecting tumors and dissociating in Cell Lytic M (Sigma; Cat# C2978) with Protease Inhibitor Cocktail (Sigma; Cat# S8820). Tumors were incubated at room temperature for 10 minutes, vortexed, and centrifuged at 10,000 × *g* to pellet DNA and cellular matter. Lysates were removed and frozen at −80°C until ELISA analysis. The following ELISA assay kits were utilized: mouse IL6 (Cat# M6000B; R&D), mouse TNFα (Cat# MTA00B; R&D), VeriKine mouse IFNβ (Cat# 42400-2; PBL Assay

Science), Mouse Inflammatory Cytokines Multi-Analyte ELISArray Kit (Cat# MEM004a; Qiagen).

Intracellular cytokine staining (ICS)

Tumors were collected at indicated time points after i.t. CDN injection in media containing Golgi inhibitors (monensin and brefeldin A) and maintained in Golgi inhibitors throughout processing. Single-cell suspensions were prepared by dissociation with scissors, then by GentleMACs, followed by incubation in 0.2% w/v collagenase IV (Worthington Biochemical) and benzonase (25 U/mL; Sigma-Aldrich) for 30 minutes at 37°C. Samples were mechanically dissociated over the GentleMACS again as before and then cultured for 4 hours. The samples were then stained for surface markers, fixed in BD Cytofix/Cytoperm (BD Biosciences; Cat# 553722) according to the manufacturer's protocol and stained for intracellular cytokines in Permwash (BD Biosciences; Cat# 554723). Samples were analyzed using an LSR II cytometer with FACSDiva software (BD Biosciences), and data were quantified using Cytobank (Cytobank, Inc.).

The following antibodies and reagents were used: from BioLegend: Ly-6G-BV510 (1A8), Ly-6C–BV711 (HK1.4), TNFα-PE (MP6-XT22), CD90.2-AF700 (30-H12); From BD: CD11b-BUV395 (M1/70), CD19-BUV737 (ID3), MHC class II-BV605 (M5), CD45-BB515 (30-F11), NK1.1-PE-CF594 (PK136), CD11c–PE-Cy7 (HL3); From PBL Assay Science: purified IFNβ (RMMB-1) conjugated with AF647 protein labeling kit (Thermo Fisher Scientific, Cat# A20186); from Thermo Fisher Scientific: Near-IR Dead cell stain (Cat# L34976).

Statistical analysis

Graphical Illustrations were created in Prism7 (Graph Pad). Statistical significance for bar graphs was determined using one- or two-tailed, unpaired Student *t* tests, also using Prism7. Statistical significance for tumor outgrowth curves was calculated by performing Student *t* tests on individual time points. *, $P < 0.05$; **, $P < 0.01$; ***, $P < 0.001$; and ****, $P < 0.0001$. ns, not significant.

Results

Intratumoral injection of CDN leads to acute rejection of B16F10 tumors

We sought to build upon our previously published results by further defining the mechanism of action at both macroscopic and microscopic levels for the acute rejection of tumors following i.t. CDN treatment. To study this, we used the CDN derivative ADU-S100 (referred to here as "CDN"). Animals were treated as in Fig. 1A. Established tumors were injected i.t. with CDN for a total of three doses. Within 48 to 72 hours of the first injection, erythema, induration, and necrosis were apparent at the injection site (Supplementary Fig. S1). By 4 to 5 days after injection, an eschar formed, and tumors were no longer palpable. Eight days after the first i.t. injection, mock-treated animals bore tumors approaching or exceeding 2,000 mm^3, necessitating sacrifice. In distinct contrast, CDN-treated mice were left with eschars remaining at the site of the initial tumor (Fig. 1B–D). Several weeks posttreatment, mice that had completely cleared tumors showed evidence of eschar healing

and injection site depigmentation, suggestive of a melanocyte-specific T-cell response (Fig. 1F). This model was dependent upon tumor volume at the time of initial treatment. Across multiple experiments, 11/14 animals bearing tumors 150 mm^3 or smaller experienced full regression of the primary tumor. By contrast, 1/5 animals with a tumor burden greater than 150 mm^3 when therapy was initiated experienced complete regression. In some instances, injection and necrosis of these rapidly growing tumors was incomplete and relapse occurred. In such cases, regrowth generally appeared near the periphery of the initial i.t. injection site (Fig. 1E, arrow notes tumor regrowth). We hypothesized that regrowth may be due to two phenomena: (i) the aggressive growth of B16F10 tumor cells or (ii) the lack of priming of an effective tumor-specific $CD8^+$ T-cell response in animals where regrowth of B16F10 was observed.

Intratumoral CDN treatment induces an acute innate immune response

To better understand the immunological effects of i.t. CDN, we performed analyses of the tumor microenvironment (TME) in treated mice. Because such treatment results in significant inflammation and necrosis within 48 to 72 hours of injection (Supplementary Fig. S1), as well ascaspase3 activation within 24 hours of injection (Fig. 2B), we hypothesized the involvement of innate responses, rather than rapid infiltration of tumors with adaptive lymphocyte populations. Utilizing the B16F10 model shown in Fig. 1, we first quantified the cellular components of the TME 24 hours after i.t. CDN treatment. Both tumors (Fig. 2) andTDLNs (Supplementary Fig. S2) were analyzed. Although innate cell subsets such as $CD11b^+F4/80^+$ macrophages and $CD11b^{hi}F4/80^-$ neutrophils increased in the TME, T and B lymphocytes were generally, though not always significantly, decreased after i.t. CDN, and NK cells in the TME were essentially unchanged following i.t. CDN treatment (Fig. 2A). TheTDLNs exhibited an analogous decrease in T cells, along with a significant increase in high FSC and SSC cells, around 40% of which were $CD11b^+F4/80^+$ macrophages (Supplementary Fig. S2A).

We next quantified i.t. (Fig. 2C) and intra-TDLN (Supplementary Fig. S2B) cytokines 1 hour and 5 hours after CDN treatment. Several innate cytokines, including GM-CSF, IL1, and TNFα, as well as chemotactic factors MCP-1 and RANTES, were increased significantly 5 hours after CDN injection. This broad-based increase in cytokines and chemokines in these compartments at the 5 hours may suggest a contribution of both direct STING signaling, as well as secondary induction of pathways activated by the initial wave of STING-induced effector molecules.

TNFα is required for maximal antitumor response to i.t. CDN

To identify the immune components critical for i.t.-CDN–mediated antitumor responses, we repeated the experiments shown in Fig. 1A using a panel of knockout mouse strains (Fig. 3A–G; Supplementary Fig. S3). As expected, whereas parental WT C57BL/6 mice exhibited complete acute control of tumors following i.t. CDN injection, $STING^{-/-}$ animals were unresponsive. The complete lack of CDN-dependent antitumor efficacy observed in $STING^{-/-}$ mice suggested that any CDN-driven signaling and downstream effects in B16F10 tumor cells themselves did not, in isolation, significantly contribute to antitumor efficacy. To confirm this observation, we incubated B16F10, MC38, CT26, or 4T1 tumor cells with CDN

(50 μg/mL; Supplementary Fig. S3). CDN treatment of cells did not affect B16F10 cell morphology (Supplementary Fig. S3A), growth kinetics (Supplementary Fig. S3B), or induce cell death in culture (Supplementary Fig. S3C). B16F10 cells were not distinct in their hypo-responsiveness to CDN. Both B16F10 cells and MC38 murine colon carcinoma cells lacked the ability to produce IFNβ after CDN exposure, in contrast to CT26 colon and 4T1 breast tumor lines (Supplementary Fig. S3D). No lines tested produced TNFα in response to CDN (Supplementary Fig. S3E). Human melanoma and breast tumor lines, shown to harbor no STING mutations and to express varying levels of STING (36, 37), were tested in a similar fashion and did not produce IFNβ after incubation with CDN for 4 and 24 hours (Supplementary Fig. S3F), suggesting that B16F10 melanoma is a representative model for human tumors by this measure.

In contrast to STING-deficient mice, tumor reduction and eschar formation following CDN i.t. therapy was indistinguishable between cGAS$^{-/-}$ and parental C57BL/6 mice, showing that direct engagement of STING by i.t. administration of CDN obviates the requirement for sensing of dsDNA by cGAS to activate the STING signaling pathway. Both RAG2$^{-/-}$ and IL6$^{-/-}$ mice also showed similar tumor necrosis and eschar formation as WT animals. Studies in IFNαR$^{-/-}$ animals were complicated by the fact that B16F10 tumors grew far more rapidly in these animals (Fig. 3G). We, thus, tested a requirement for IFN signaling by injecting CDN into non-tumor-bearing animals. We observed normal eschar formation (Fig. 3H), suggesting that, although IFN signaling is clearly important in tumor outgrowth, it may not be required for CDN activity. The only two knockout strains in which CDN activity was clearly attenuated or absent were the STING$^{-/-}$ and TNFα$^{-/-}$ animals (Fig. 3E). To confirm a requirement for TNFα in CDN-mediated antitumor responses, we treated WT C57BL/6 mice with CDN in the presence of a soluble TNF-RII fusion protein that effectively blocks TNFα signaling (ref. 38; Enbrel; Amgen; Fig. 3I). These results were consistent with the results seen in TNFα knockout animals—treatment with CDN alone resulted in tumor clearance in 5/8 mice, but when combined with TNFα blockade, tumors progressed in all eight animals in that cohort. TNFα blockade in 4T1, CT26, and MC38 tumor models dramatically reduced the size of observable eschars after CDN administration. The reduction in necrosis was not as complete as in TNFα KO mice, suggesting that TNFα blockade by this measure incompletely neutralizes the cytokine. In mice-bearing CT26, MC38, or 4T1 tumors, high-dose i.t. ADU-S100-driven tumor clearance was not significantly impacted by TNFα blockade, although acute necrosis was attenuated (Supplementary Fig. S4A and S4B). These data provide evidence that the requirement for TNFα may differ between tumor types.

Bone marrow-produced TNFα predominates in the TME

To determine the cellular source of TNFα induced by i.t. CDN treatment, we generated a series of bone marrow chimera mice by irradiating WT C57BL/6 or TNFα$^{-/-}$ host animals and reconstituting mice with either WT or TNFα$^{-/-}$ bone marrow. The results of these studies showed that animals reconstituted with WT bone marrow, in either WT or TNFα$^{-/-}$ hosts, responded more robustly to i.t. CDN as compared with mice reconstituted with TNFα$^{-/-}$ bone marrow. Both WT and TNFα$^{-/-}$ hosts reconstituted with WT bone marrow cleared tumors efficiently (Fig. 4A). Consistent with this observation, mice harboring WT bone

marrow had significantly higher i.t. TNFα compared with their counterparts reconstituted with TNFα$^{-/-}$ bone marrow. The TME of animals with TNFα$^{-/-}$ bone marrow did not express detectable TNFα 24 hours after CDN i.t. therapy (Fig. 4B). However, some necrosis and inhibition of tumor outgrowth was observed in WT chimeric animals with TNFα$^{-/-}$ bone marrow, suggesting that stromal cells also have the ability to influence tumor inflammation and clearance to some degree. Taken together, these results demonstrate the importance of TNFα produced by both stromal and bone marrow compartments in response to activation of STING for optimal acute tumor clearance following i.t. CDN injection.

Innate immune cells produce TNFα and IFNβ post i.t. CDN

To understand the cellular source of innate cytokines in TME, we treated B16F10 tumor-bearing animals with 100 μg CDN i.t. and performed intracellular staining (ICS). Because bone marrow-derived cells were required for TNFα production (Fig. 4), analyses were restricted to the CD45^{+} leukocyte compartment. To ensure that we were observing primary and direct effects of CDN ligation of STING within these cells and not secondary effects from cytokine-induced downstream interferon-stimulated genes, TNFα and IFNβ levels within tumor infiltrates were assessed at early time points, i.e., at 1 hour and 5 hours post i.t. CDN injection (Fig. 5A). Within 1 hour after CDN administration, both TNFα and IFNβ were expressed by CD45^{+} cells in the TME (Fig. 5B and C). By 5 hours after injection, both TNFα and IFNβ in the CD45^{+} compartment were reduced to near background levels. Using surface markers to determine the lineage of cytokine-producing cells, we found activated monocytic cells (CD11b^{+}Ly6C^{+}MHCII^{+}) were largely responsible for production of TNFα and IFNβ, although other monocytic cells (CD11b^{+}Ly6C^{+}MHCII^{-}), aswell as macrophages (CD11C^{+}CD11b^{+}MHCII^{+}), also contributed to production of these cytokines (Fig. 5C). Consistent with our prior data, theTME contained very few T and B cells at these early time points.

Stromal STING signaling contributes to injection site necrosis

Because the results from our bone marrow chimera studies indicated that neither TNFα competent bone marrow-derived cells or stromal cells alone were sufficient to fully recapitulate the phenotype of the acute antitumor response to CDN treatment into WT animals, we sought to better define the relative contributions of these two compartments. To address this question, we made a series of bone marrow chimeras using WT and STING$^{-/-}$ mouse strains. WT and STING$^{-/-}$ hosts were first irradiated and then reconstituted with either WT or STING$^{-/-}$ bone marrow cells. B16F10 tumor cells were implanted into chimeric and parental mice, and CDN was given by i.t. injection when tumors were well established. After CDN therapy, tumor outgrowth was inhibited in all mice except in STING$^{-/-}$ parental mice (Fig. 6A and B). Treatment in both chimeric groups (STING$^{-/-}$ bone marrow into WT and WT bone marrow into STING$^{-/-}$ mice) resulted in similar reduction of tumor burden. As we observed in studies with the TNFα$^{-/-}$ chimeric mice, only WT bone marrow into WT animals could completely reject tumors, whereas all chimeric animals exhibited partial reductions and eventually succumbed to tumor burden. However, only animals with STING signaling competent stroma (WT animals with STING$^{-/-}$ or WT bone marrow) became necrotic afteri.t. CDN treatment (Fig. 6C). In distinct contrast, necrosis was not observed in any animal that lacked stromal STING signaling (STING$^{-/-}$ animals with

STING^−^ or WT bone marrow), as determined either by visualization (Fig. 6C) or by blind scoring of photographs for necrosis signatures (Fig. 6D). Consistent with this observation, significant CDN-induced expression of IFNβ, IL6, and TNFα were measured by ELISA 24 hours after i.t. injection only in tumor lysates processed from mice with intact stromal STING signaling (Fig. 6E). These data reveal that although CDNs elicit cellular responses from both bone marrow and stromal compartments, a qualitatively different response occurs when the stroma is activated, leading to injection site necrosis.

APC activation by stromal or hematopoietic STING signaling

In prior studies, we found that i.t. administration of CDNs can enhance tumor-specific adaptive responses, and animals that clear tumors can reject a future tumor rechallenge (35). Confirming a putative downstream adaptive immune response, we found that i.t. treatment with CDNs can result in vitiligo (Fig. 1F). To address the role of STING signaling in DC activation in the hematopoietic and stromal compartments, we again generated WT and $STING^{-/-}$ chimeric mice (Fig. 6) and analyzed the composition and relative APC activation in those animals. A significant infiltration of FSC^{hi} SSC^{hi} cells, corresponding to macrophage and monocyte populations, into the TDLNs was noted in all chimeric mice that were evaluated, except for $STING^{-/-}$ mice with $STING^{-/-}$ bone marrow (Fig. 7A). FSC^{hi} SSC^{hi} cells were further defined using the lineage markers CD11b and CD11c to identify both macrophage and dendritic cell populations (Fig. 7B). Both $CD11b^{+}CD11c^{+}$ and $CD11b^{Lo}CD11c^{+}$ macrophage and DC populations, as well as $CD11b^{+}CD11c^{-}$ neutrophils were enriched in the TDLNs 24 hours after CDN administration (Fig. 7C). In all chimeras except for $STING^{-/-}$ mice with $STING^{-/-}$ bone marrow, upregulation of the costimulatory molecule CD86 on macrophage and DC populations was observed after CDN administration (Fig. 7D). These results suggest that i.t. CDN can result in activation of APCs either via direct activation of the STING pathway in APCs, or, alternatively, indirectly through the production of inflammatory cytokines by STING competent stroma.

Discussion

We show here that i.t. administration of CDN is a powerful immunotherapy that results in tumor clearance and long-term survival of animals bearing aggressive B16F10 tumors. In these studies, we focused on the acute effects of high-dose i.t. injection CDN therapy, while also noting the potential for APC activation and long-term adaptive immunity. Our bone marrow chimera studies showed that both bone marrow-derived and stromal cells are important in tumor clearance, and neither compartment alone is sufficient for full tumor clearance. These studies represent important progress toward understanding the effects of CDN on immune and nonimmune cell subsets.

I.t. administration of CDN results in significant changes in the TME. Flow cytometry revealed an initial reduction in the proportion of tumor-infiltrating lymphocytes and simultaneous acute increase of tumor-infiltrating macrophages and neutrophils. The tumor cells themselves undergo cell death, as demonstrated by robust IHC staining for cleaved caspase 3 in the tumor. This change in cellular composition is likely both a product of and a cause of the significant increase in multiple i.t. cytokines, including IL6, TNFα, IFNβ, and

GM-CSF. This cytokine increase has been reported previously and is hypothesized to be the result of both NF-κB and IRF-3 activity, as well as STAT6 (14, 15). However, whether NF-κB activation is a direct result of STING ligation or rather the result of secondary cytokine signaling remains unclear and is a difficult hypothesis to address due to the rapid induction and abundance of cytokines observed after CDN administration. A report by Gaidt and colleagues showed that the DNA inflammasome is one of the downstream targets of STING activation, leading to IL1 β and IP-10 secretion (39).

The data shown here emphasize the potent, ablative effect of high concentrations of innate cytokines induced by CDNs in TME. Studies have shown that IFNαR signaling is an important mediator of antitumor immunity (40), and although our experiments suggested that the acute necrosis following i.t. administration of CDN is not IFNαR mediated, further studies in our lab, as well as in other groups, have shown that IFNαR$^{-/-}$ animals have reduced capacity to mount long-term immune responses after CDN therapy (33, 35).

Mice lacking TNFα did not develop injection site necrosis when CDN were administered i.t. These findings were corroborated in our studies showing that tumor necrosis can be significantly reduced by administration of the TNFα inhibitor Enbrel. TNFα blockade reduced both the size of the eschar at the injection site, as well as tumor clearance in the nonimmunogenic B16F10 model. In the MC38, CT26, and 4T1 tumor models, TNFα blockade reduced the size of the eschar but did not attenuate tumor clearance. This suggests that there may be distinct phases of antitumor immunity generated by i.t. CDN therapy. TNFα is likely required for acute necrosis, whereas the chronic nature of a tumor burden may require the induction of adaptive immunity for an antitumor effect. We suspect that the difference in tumor rejection between B16F10 and MC38, CT26, and 4T1 models is due to differences in immunogenicity among these tumor lines. At baseline, B16F10 tumors are generally immunologically bland, and this lack of inherent immunogenicity is reflected in the inability of PD-1 or PD-L1 blockade to attenuate tumor growth (41, 42). By comparison, MC38, 4T1, and CT26 tumors are variably infiltrated with a more immunogenic signature (43). As a result, CDN treatment of B16F10 tumors may be hampered by the lack of a preexisting adaptive immune response and, thus, is more reliant on innate mechanisms. Therefore, whereas the acute induction of TNFα by i.t. CDNs is necessary for the clearance of the nonimmunogenic B16F10 tumor line, more immunogenic models may not require such TNFα-mediated tumor destruction for clearance. Instead, TNFα independent mechanisms are sufficient to clear tumors.

We were further able to dissect the TNFα-producing bone marrow-derived populations using linage markers and multidimensional flow cytometry. Using this approach, we ascertained that although multiple lineages of bone marrow-derived cells were capable of producing TNFα, monocytes and macrophages were both more likely to be producing TNFα, based on the frequency of cells positive for TNFα and TNFα MFI. Although these results indicate that innate immune signaling from high-dose CDN can clear tumors in the absence of the adaptive immune system, it is clear that adaptive immunity is critical for long-term efficacy of CDN therapy on the whole and in response to lower dose administrations of CDN.

With this comprehensive study of the critical cellular components and cytokines induced by acute CDN treatment, it has become abundantly clear that the CDN-dependent immune clearance of tumors depends on cross-talk or additive effects from both immune and stromal cells. At first glance, it may seem that the importance of TNFα production by bone marrow-derived cells is not reconcilable with our data that show STING competence in the stroma is necessary. However, it is conceivable that STING signaling in the stroma leads to production of factors that attract bone marrow cells, potentiate their production of TNFα in the tumor, or that STING signaling primes the TME for destruction by upregulation of TNFαR1. Future studies will be required to elucidate these mechanisms and to understand the bone marrow and stromal STING requirements for priming adaptive immune responses by i.t. CDN administration.

As cancer immunotherapies are being approved for treatment for a variety of indications, it is important to recognize the impact on stromal cells, as well as immune cells within tumors. In mice and in humans, stromal cells, such as fibroblasts and endothelial cells, can express and signal through PRRs, shaping the immune response through production of cytokines. In our models, CDN injection acutely leads to the activation of the stroma, an inflammatory immune environment, and tumor clearance. Activation of APCs and observations of long-term vitiligo at injection sites suggest that tumor-specific adaptive responses exist and are functional. The direct injection of CDN is a powerful means to target TME reorganization and the induction of functional immune responses to cancer through activation of STING signaling in stromal and immune cells within the tumor.

Supplementary Material

Refer to Web version on PubMed Central for supplementary material.

Acknowledgments

These studies were supported by NIH/NCI R01CA154555, the Prostate Cancer Foundation (PCF), The Patrick C. Walsh Fund and a sponsored research agreement from Aduro Biotech.

The authors of this article would like to thank Ada Tam and Lee Blosser for their help and maintenance of the flow cytometry core. We would also like to thank Dr. Young Kim for his donation of Golden Ticketmice, and Dr. Skip Virgin for his donation of cGAS$^{-/-}$ mice.

The costs of publication of this article were defrayed in part by the payment of page charges. This article must therefore be hereby marked *advertisement* in accordance with 18 U.S.C. Section 1734 solely to indicate this fact

References

1. Hayashi F, Smith KD, Ozinsky A, Hawn TR, Yi EC, Goodlett DR, et al. The innate immune response to bacterial flagellin is mediated by Toll-like receptor 5. Nature 2001;410:1099–103. [PubMed: 11323673]
2. Hoshino K, Takeuchi O, Kawai T, Sanjo H, Ogawa T, Takeda Y, et al. Cutting edge: Toll-like receptor 4 (TLR4)-deficient mice are hyporesponsive to lipopolysaccharide: Evidence for TLR4 as the Lps gene product. J Immunol 1999;162:3749–52. [PubMed: 10201887]
3. O'Neill LA, Golenbock D, Bowie AG. The history of Toll-like receptors redefining innate immunity. Nat Rev Immunol 2013;13:453–60. [PubMed: 23681101]
4. Akira S, Takeda K. Toll-like receptor signalling. Nat Rev Immunol 2004;4:499–511. [PubMed: 15229469]

5. Sun L,Wu J,Du F, Chen X, Chen ZJ. Cyclic GMP-AMP synthase is a cytosolic DNA sensor that activates the type I interferon pathway. Science 2013;339:786–91. [PubMed: 23258413]
6. Ablasser A, Goldeck M, Cavlar T, Deimling T, Witte G, Rohl I, et al. cGAS produces a 2′–5′-linked cyclic dinucleotide second messenger that activates STING. Nature 2013;498:380–4. [PubMed: 23722158]
7. Barber GN. STING-dependent cytosolic DNA sensing pathways. Trends Immunol 2014;35:88–93. [PubMed: 24309426]
8. Jin L, Waterman PM, Jonscher KR, Short CM, Reisdorph NA, Cambier JC. MPYS, a novel membrane tetraspanner, is associated with major histocompatibility complex class II and mediates transduction of apoptotic signals. Mol Cell Biol 2008;28:5014–26. [PubMed: 18559423]
9. Ishikawa H, Barber GN. Sting is an endoplasmic reticulum adaptor that facilitates innate immune signaling. Nature 2008;455:674–8. [PubMed: 18724357]
10. Wu J, Sun L, Chen X, Du F, Shi H, Chen C, et al. Cyclic GMP-AMP is an endogenous second messenger in innate immune signaling by cytosolic DNA. Science 2013;339:826–30. [PubMed: 23258412]
11. Sun WX, Li Y, Chen L, Chen HH, You FP, Zhou X, et al. ERIS, an endoplasmic reticulum IFN stimulator, activates innate immune signaling through dimerization. Proc Natl Acad Sci USA 2009;106:8653–8. [PubMed: 19433799]
12. Konno H, Konno K, Barber GN. Cyclic dinucleotides trigger ULK1 (ATG1) phosphorylation of STING to prevent sustained innate immune signaling. Cell 2013;155:688–98. [PubMed: 24119841]
13. Ishikawa H,Ma Z, Barber GN. Sting regulates intracellular DNA-mediated, type I interferon-dependent innate immunity. Nature 2009;461:788–92. [PubMed: 19776740]
14. Abe T, Harashima A, Xia T, Konno H, Konno K, Morales A, et al. STING recognition of cytoplasmic DNA instigates cellular defense. Mol Cell 2013; 50:5–15. [PubMed: 23478444]
15. Chen HH, Sun H, You FP, Sun WX, Zhou X, Chen L, et al. Activation of STAT6 by STING is critical for antiviral innate immunity. Cell 2011; 147:436–46. [PubMed: 22000020]
16. Sauer JD, Sotelo-Troha K, von Moltke J, Monroe KM, Rae CS, Brubaker SW, et al. The N-ethyl-N-nitrosourea-induced goldenticket mouse mutant reveals an essential function of sting in the in vivo interferon response to Listeria monocytogenes and cyclic dinucleotides. Infect Immun 2011;79:688–94. [PubMed: 21098106]
17. Jin L, Hill KK, Filak H, Mogan J, Knowles H, Zhang BC, et al. MPYS is required for ifn response factor 3 activation and type I IFN production in the response of cultured phagocytes to bacterial second messengers cyclicdi-AMP and cyclic-di-GMP. J Immunol 2011;187:2595–601. [PubMed: 21813776]
18. Archer KA, Durack J, Portnoy DA. STING-dependent type I IFN production inhibits cell-mediated immunity to Listeria monocytogenes. PLoS Pathog 2014;10:e1003861. [PubMed: 24391507]
19. Yang K, Wang J, Wu M, Li M, Wang Y, Huang X. Mesenchymal stem cells detect and defend against gamma herpesvirus infection via the cGAS–STING pathway. Sci Rep 2015;5:7820. [PubMed: 25592282]
20. Sun L, Xing Y, Chen X, Zheng Y, Yang Y, Nichols DB, et al. Coronavirus papain-like proteases negatively regulate antiviral innate immune response through disruption of STING-mediated signaling. PLoS One 2012;7:e30802. [PubMed: 22312431]
21. Sze A, Belgnaoui SM,Olagnier D, Lin RT, Hiscott J, van Grevenynghe J. Host restriction factor SAMHD1 limits human T cell leukemia virus type 1 infection of monocytes via STING-mediated apoptosis. Cell Host Microbe 2013;14:422–34. [PubMed: 24139400]
22. Dai PH, Wang WY, Cao H, Avogadri F, Dai LP, Drexler I, et al. Modified vaccinia virus Ankara triggers type I IFN production in murine conventional dendritic cells via a cGAS/STING-mediated cytosolic DNA-sensing pathway. PLoS Pathog 2014;10:13.
23. Guo HT, Koenig R, Deng M, Riess M, Mo JY, Zhang L, et al. NLRX1 sequesters STING to negatively regulate the interferon response, thereby facilitating the replication of HIV-1 and DNA viruses. Cell Host Microbe 2016;19:515–28. [PubMed: 27078069]

24. Trotard M, Tsopoulidis N, Tibroni N, Willemsen J, Binder M, Ruggieri A, et al. Sensing of HIV-1 infection in Tzm-bl cells with reconstituted expression of STING. J Virol 2016;90:2064–76. [PubMed: 26656698]
25. Chen Q, Boire A, Jin X, Valiente M, Er EE, Lopez-Soto A, et al. Carcinomaastrocyte gap junctions promote brain metastasis by cGAMP transfer. Nature 2016;533:493–8. [PubMed: 27225120]
26. Ablasser A, Schmid-Burgk JL,Hemmerling I, Horvath GL, Schmidt T, Latz E, et al. Cell intrinsic immunity spreads to bystander cells via the intercellular transfer of cGAMP. Nature 2013;503:530–4. [PubMed: 24077100]
27. Woo SR, Fuertes MB, Corrales L, Spranger S, Furdyna MJ, Leung MY, et al. STING-dependent cytosolic DNA sensing mediates innate immune recognition of immunogenic tumors. Immunity 2014;41:830–42. [PubMed: 25517615]
28. Downey CM, Aghaei M, Schwendener RA, Jirik FR. DMXAA causes tumor site-specific vascular disruption in murine non-small cell lung cancer, and like the endogenous non-canonical cyclic dinucleotide STING agonist, 2′ 3′-cGAMP, induces M2 macrophage repolarization. PLoS One 2014;9:14.
29. Baird JR, Friedman D, Cottam B, Dubensky TW, Kanne DB, Bambina S, et al. Radiotherapy combined with novel STING-targeting oligonucleotides results in regression of established tumors. Cancer Res 2016;76:50–61. [PubMed: 26567136]
30. Dubensky TW, Jr., Kanne DB, Leong ML. Rationale, progress and development of vaccines utilizing STING-activating cyclic dinucleotide adjuvants. Ther Adv Vacc 2013;1:131–43.
31. Fu J, Kanne DB, Leong M, Glickman LH, McWhirter SM, Lemmens E, et al. STING agonist formulated cancer vaccines can cure established tumors resistant to PD-1 blockade. Sci Transl Med 2015;238ra52.
32. Ohkuri T, Ghosh A, Kosaka A, Zhu JZ, Ikeura M, David M, et al. STING contributes to antiglioma immunity via triggering Type I IFN signals in the tumor microenvironment. Cancer Immunol Res 2014;2:1199–208. [PubMed: 25300859]
33. Chandra D, Quispe-Tintaya W, Jahangir A, Asafu-Adjei D, Ramos I, Sintim HO, et al. STING ligand c-di-GMP improves cancer vaccination against metastatic breast cancer. Cancer Immunol Res 2014;2:901–10. [PubMed: 24913717]
34. Deng L, Liang H, Xu M, Yang X, Burnette B, Arina A, et al. STING-dependent cytosolic DNA sensing promotes radiation-induced type I interferondependent antitumorimmunity inimmunogenic tumors. Immunity 2014; 41:843–52. [PubMed: 25517616]
35. Corrales L,Glickman LH, McWhirter SM, Kanne DB, Sivick KE, Katibah GE, et al. Direct activation of STING in the tumor microenvironment leads to potent and systemic tumor regression and immunity. Cell Rep 2015; 11:1018–30. [PubMed: 25959818]
36. Reinhold WC, Sunshine M, Liu H, Varma S, Kohn KW, Morris J, et al. CellMiner: a web-based suite of genomic and pharmacologic tools to explore transcript and drug patterns in the NCI-60 cell line set. Cancer Res 2012;72:3499–511. [PubMed: 22802077]
37. Xia T, Konno H, Barber GN. Recurrent loss of STING signaling in melanoma correlates with susceptibility to viral oncolysis. Cancer Res 2016; 76:6747–59. [PubMed: 27680683]
38. Liu R, Bal HS, Desta T, Behl Y, Graves DT. Tumor necrosis factor-alpha mediates diabetes-enhanced apoptosis of matrix-producing cells and impairs diabetic healing. Am J Pathol 2006;168:757–64. [PubMed: 16507891]
39. Gaidt MM, Ebert TS, Chauhan D, Ramshorn K, Pinci F, Zuber S, et al. The DNA inflammasome in human myeloid cells is initiated by a STINGcell death program upstream of NLRP3. Cell 2017;171:1110–24. [PubMed: 29033128]
40. Yang XM, Zhang XM, FuML Weichselbaum, Gajewski TF, Guo YJ, et al. Targeting the tumor microenvironment with interferon-beta bridges innate and adaptive immune responses. Cancer Cell 2014;25:37–48. [PubMed: 24434209]
41. Twyman-Saint Victor C, Rech AJ,Maity A, Rengan R, Pauken KE, Stelekati E, et al. Radiation and dual checkpoint blockade activate non-redundant immune mechanisms in cancer. Nature 2015;520:373–7. [PubMed: 25754329]
42. Selby MJ, Engelhardt JJ, Johnston RJ, Lu LS, Han M, Thudium K, et al. Preclinical development of ipilimumab and nivolumab combination immunotherapy: mouse tumor models, in vitro

functional studies, and cynomolgus macaque toxicology. PLoS One 2016;11:e0161779. [PubMed: 27610613]

43. Lechner MG, Karimi SS, Barry-Holson K, Angell TE, Murphy KA, Church CH, et al. Immunogenicity of murine solid tumor models as a defining feature of in vivo behavior and response to immunotherapy. J Immunother 2013;36:477–89. [PubMed: 24145359]

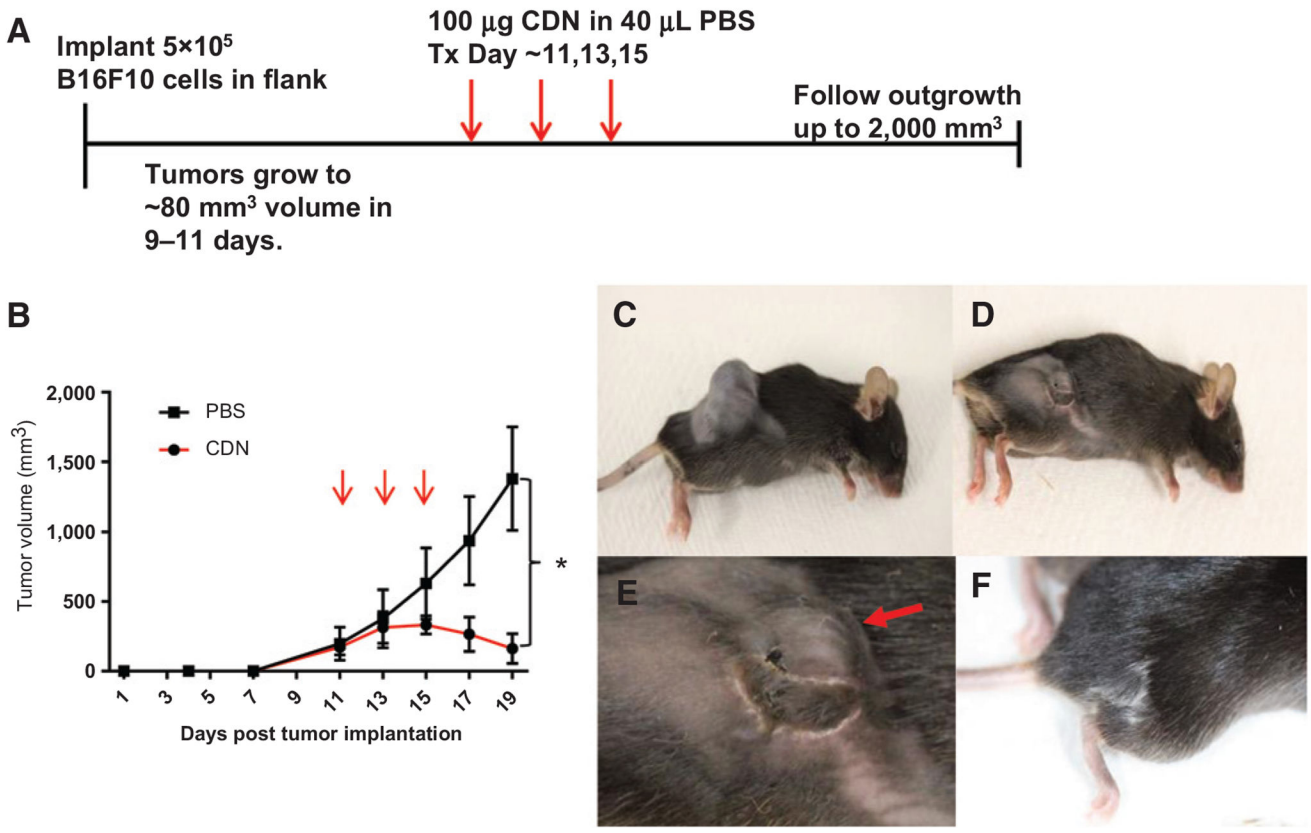

Figure 1.

Therapeutic i.t. injection of CDN leads to acute rejection of B16F10 melanoma. **A,** Treatment schematic for i.t. injection of tumors. Mice were implanted with 5×10^5 B16F10 on day 0, then assessed for tumor volume until the group averaged ~80 mm^3. At that time, mice were treated with 100 µg CDN in 40 µL PBS, or with PBS alone every other day for a total of three treatments (red arrows). **B,** Tumor outgrowth of B16F10-bearing animals treated as described in **A**. Representative of >3 experiments with ≥3 animals each. Red arrows indicate time of treatment. Error bars represent SEM and *P* value was calculated by an unpaired *T* test of volumes on day 19. *, $P < 0.05$. **C**-**F**, Representative pictures of mice from experiments shown in **B**. Mock-treated (**C**) or CDN-treated (**D, E** close-up; arrow indicates regrowth) animals 9 days after treatment or 3+ weeks after treatment (**F**), when surviving mice show injection site vitiligo.

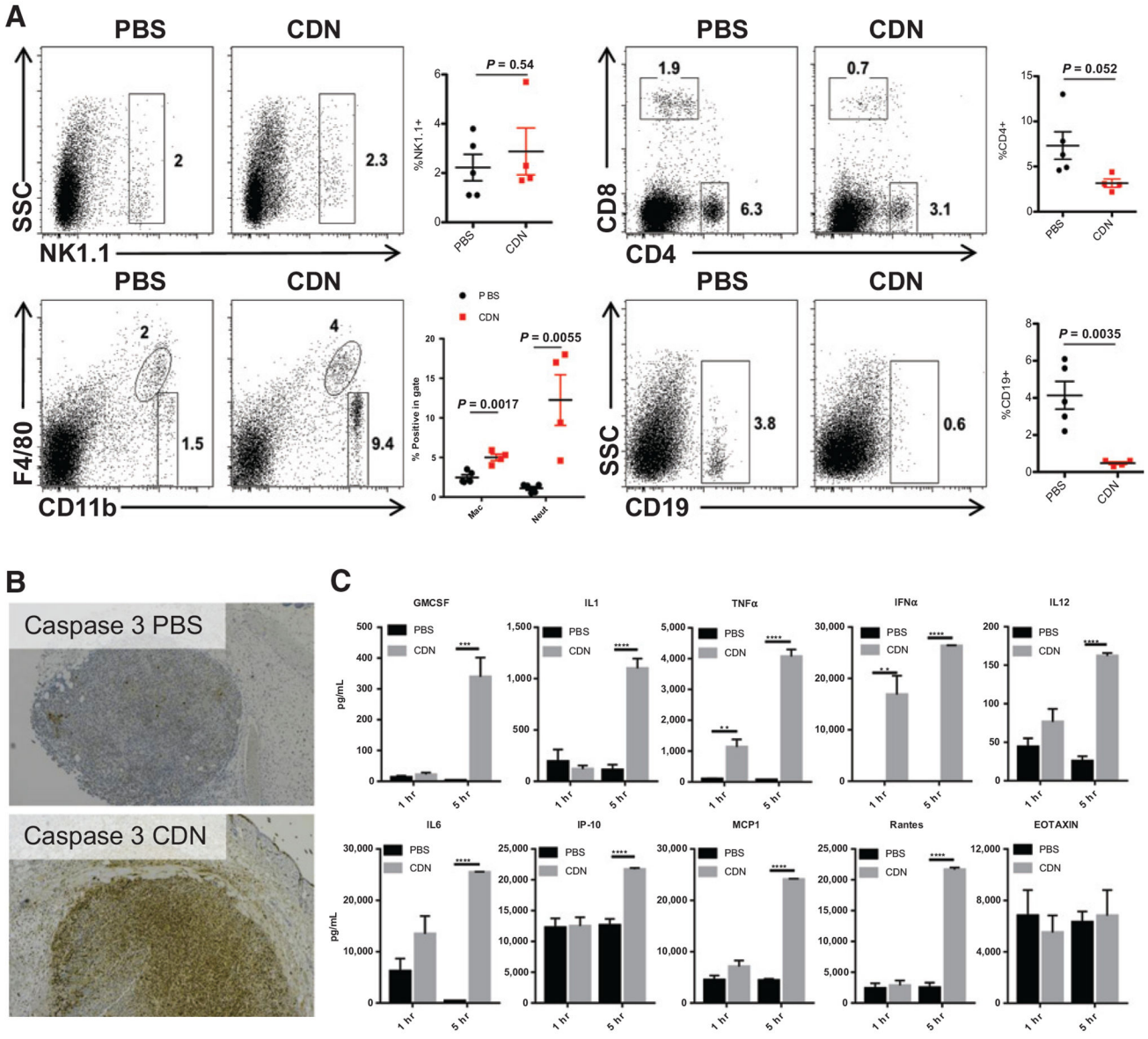

Figure 2.

CDN injection causes a distinct cytokine and cellular profile in the tumor. **A,** Flow cytometry of B16F10 tumors 24 hours after a single 100 μg i.t. CDN dose. Dead cells were excluded with viability dye gate, and cellular debris was excluded with FSC/SSC gate. Error bars represent SEM and P values were calculated by unpaired *T* tests. Graphs are representative plots of three experiments with ≥3 animals each. **B,** IHC for Caspase 3. Tumors were excised and fixed 24 hours after one dose with 100 μg i.t. CDN treatment. Representative sections shown at 4× magnification. **C,** Tumor lysate cytokines. Lysates were taken 1 and 5 hours after i.t. CDN and cytokines quantified by Luminex. Graphs are representative of two experiments with five animals each. Error bars represent SEM. *, $P < 0.05$; **, $P < 0.01$; ***, $P < 0.001$; and ****, $P < 0.0001$.

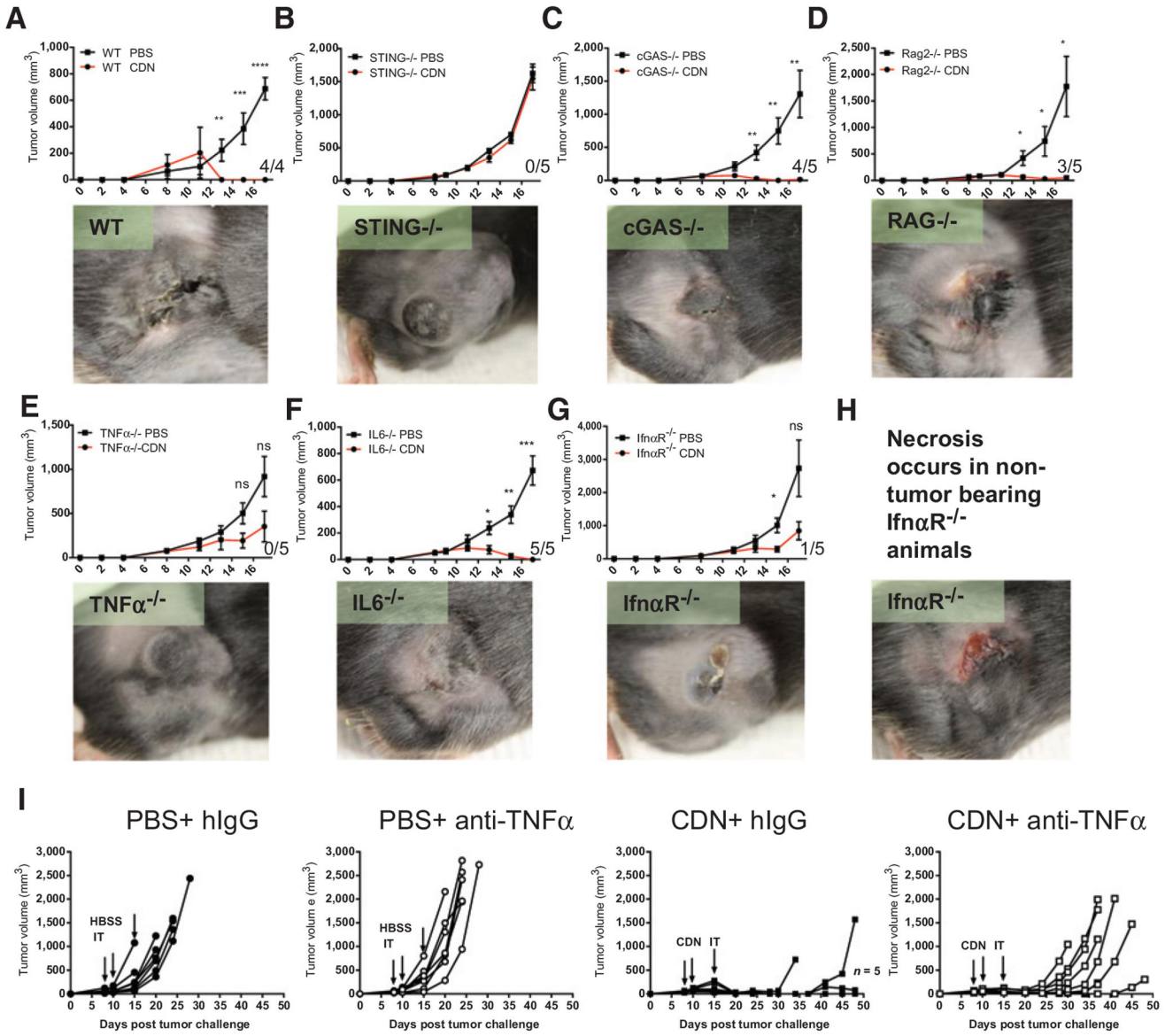

Figure 3.

TNFα is necessary for CDN-induced tumor necrosis. **A-G,** Tumor outgrowth in i.t. CDN-treated mice. Experiments were performed as in Fig. 1A. Images were acquired 6 days after initial CDN injection. The fraction of animals experiencing complete responses (tumor regression to 0 mm^3) are noted in the bottom right inset fraction on each graph. WT group started with five animals, and one succumbed to anesthetic used for photography during the course of treatment. *, $P < 0.05$; **, $P < 0.01$; ***, $P < 0.001$; and ****, $P < 0.0001$. ns, not significant. Graphs are representative of two experiments with five animals each. **H**, i.t. injection of nontumor-bearing IfnαR$^{-/-}$ animals. **I**, WT C57BL/6 mice were inoculated 2 × 10^5 B16F10 cells in the right flank on day 0 ($n = 8$). When tumor volumes were 40 mm^3 (4–6 mm), they received three 100 μg i.t. doses of CDN or HBSS as control (days 8,10, and 15, indicated by arrows). Tumor measurements were taken twice weekly. Mice were

administered 200 μg s.c. doses of the TNFα inhibitor etanercept (Enbrel) or hIgG control on days 3, 7, 9, and 14. Results are shown as individual tumor growth curves. Data are representative of two independent experiments.

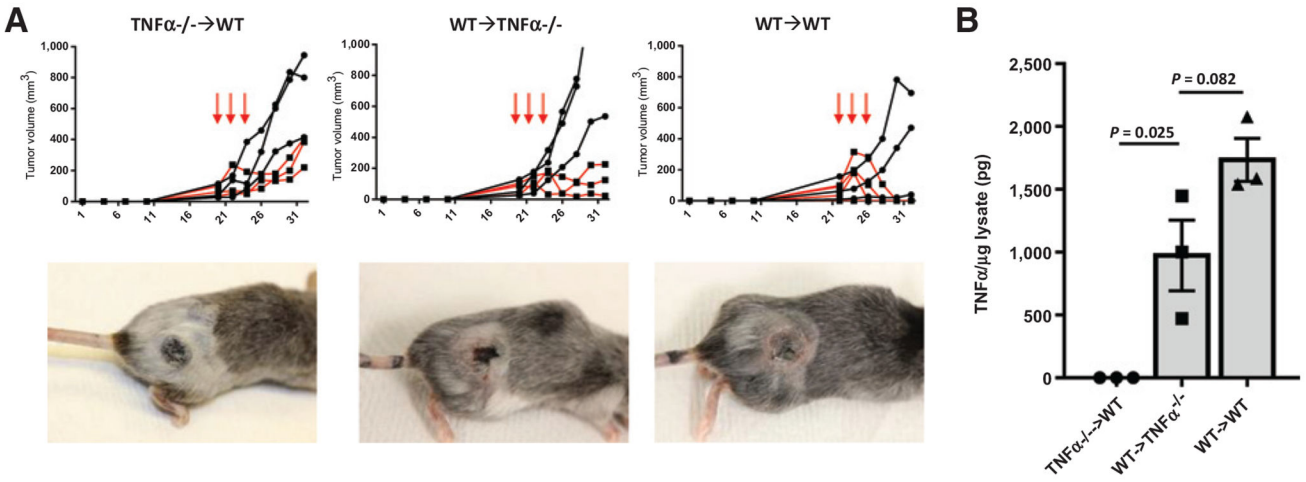

Figure 4.

Hematopoietic cell TNFα production dominates the TME. **A,** Tumor outgrowth in chimeric mice. WT and TNFα$^{-/-}$ animals were irradiated and reconstituted as indicated such that TNFα$^{-/-}$ →WT refers to TNFα$^{-/-}$ bone marrow transferred into a WT recipient. At 5+ weeks after chimerism, 5 × 10^5 B16F10 cells were implanted, and mice were treated with i.t. CDN as in Fig. 1. Graphs and photographs are representative of one experiment with three mice per group. Red arrows indicate time of treatment. **B,** Cytokine production post CDN treatment for animals in **A**. *N* = 3 animals/group, repeated once. Data were normalized to total protein concentration in lysate to correct for tumor volume. Error bars represent SEM.

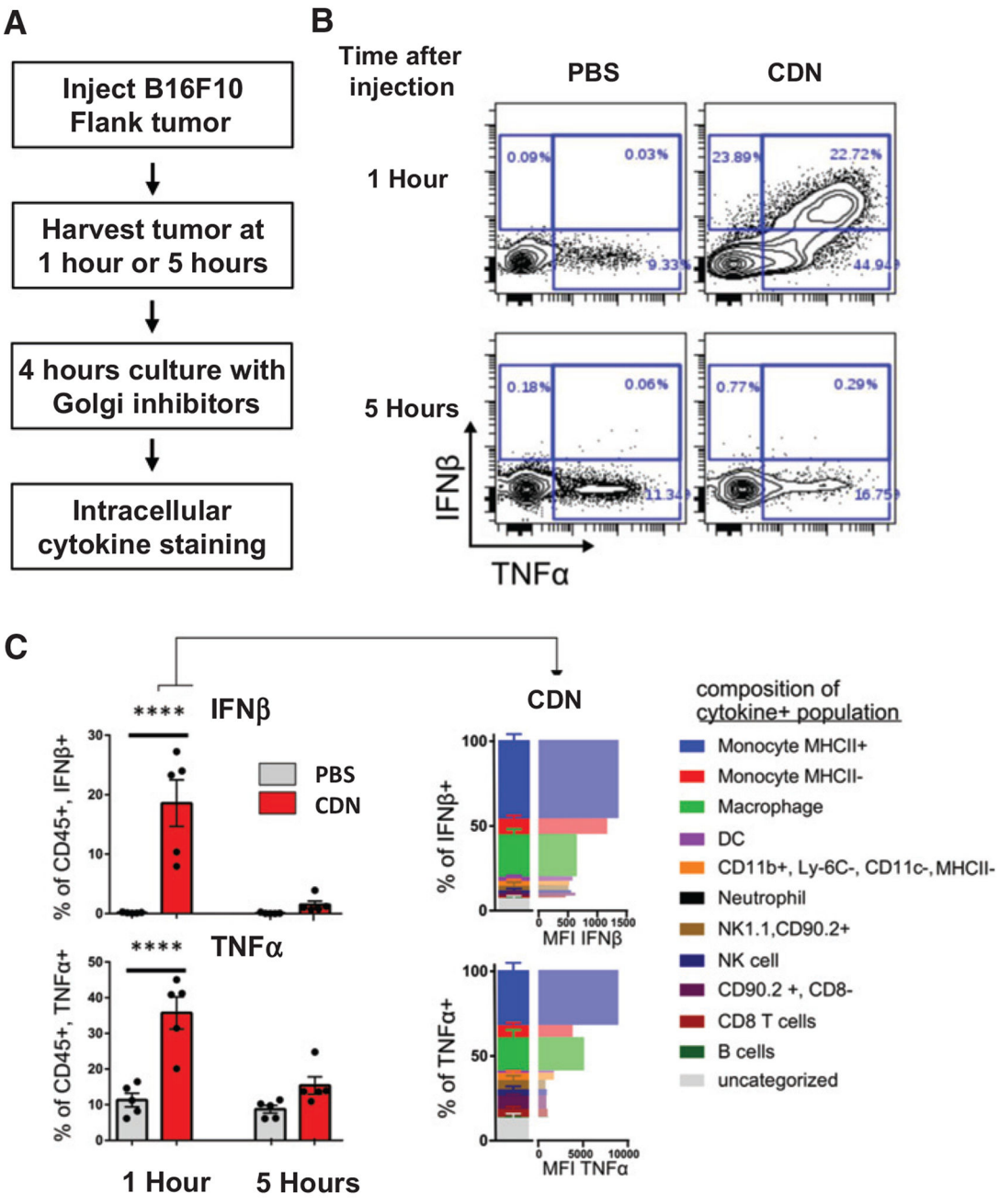

Figure 5.

Activation signature within the TME highlights the importance of bone marrow-derived cells. **A,** Experimental design. B16F10-bearing animals were injected 100 μg CDN or PBS. One or five hours after injection, tumors were processed in brefeldin A and incubated for 4 hours before ICS and analysis by flow cytometry. Results are representative of two experiments with five animals each. **B,** Representative flow plots showing IFNβ and TNFα staining in the monocyte MHCII^{+} population (CD11b^{+}Ly6C^{+}MHCII^{+}). **C,** Analysis of flow plots in **A**. Left: cytokine production from CD45^{+} cells. Right: analysis of cytokine-

producing cells. Legend on right. Results are representative of two experiments with five animals each. Error bars represent SEM. ****, $P < 0.0001$.

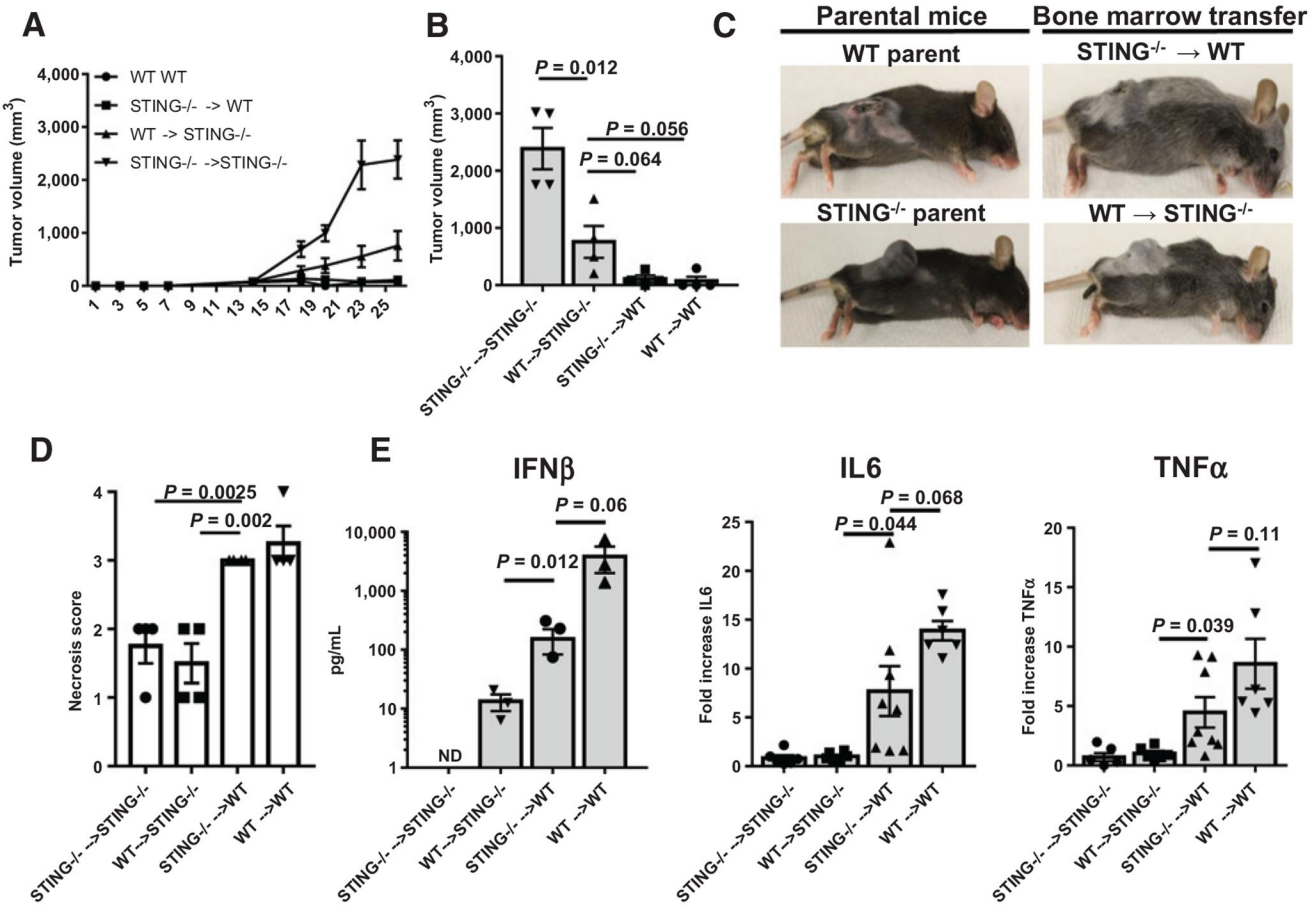

Figure 6.

Bone marrow-stromal cell STING competence is required for injection site necrosis. Outgrowth (**A**) and day 26 tumor volume comparison (**B**) of STING chimeric animals. WT and STING$^{-/-}$ animals were irradiated, chimerized, and left to recover. At 5+ weeks after chimerism, 5×10^5 B16F10 cells were implanted, and mice were treated with i.t. CDN as in Fig. 1. Data are representative of three independent experiments with independently generated chimeric mice, ≥3 mice per group. **C,** Photographs of treated chimeric and parental animals. Taken 8 days after CDN injection. **D,** Necrosis scoring for chimeric animals. Photographs were visually analyzed in a blinded manner. **E,** ELISAs of chimeric animal tumor lysate. For IL6 and TNFα, values from ELISA plates were then normalized to total protein content of lysate, then to WT→STING cytokine production. Data points are from two independent experiments, with 3 to 4 biological replicate animals per group, per experiment. For IFNβ, data points are from one experiment with three biological replicates, representative of two independent experiments. Fold changes from these independent experiments were not identically aligned, so graph points were not combined. All error bars represent SEM.

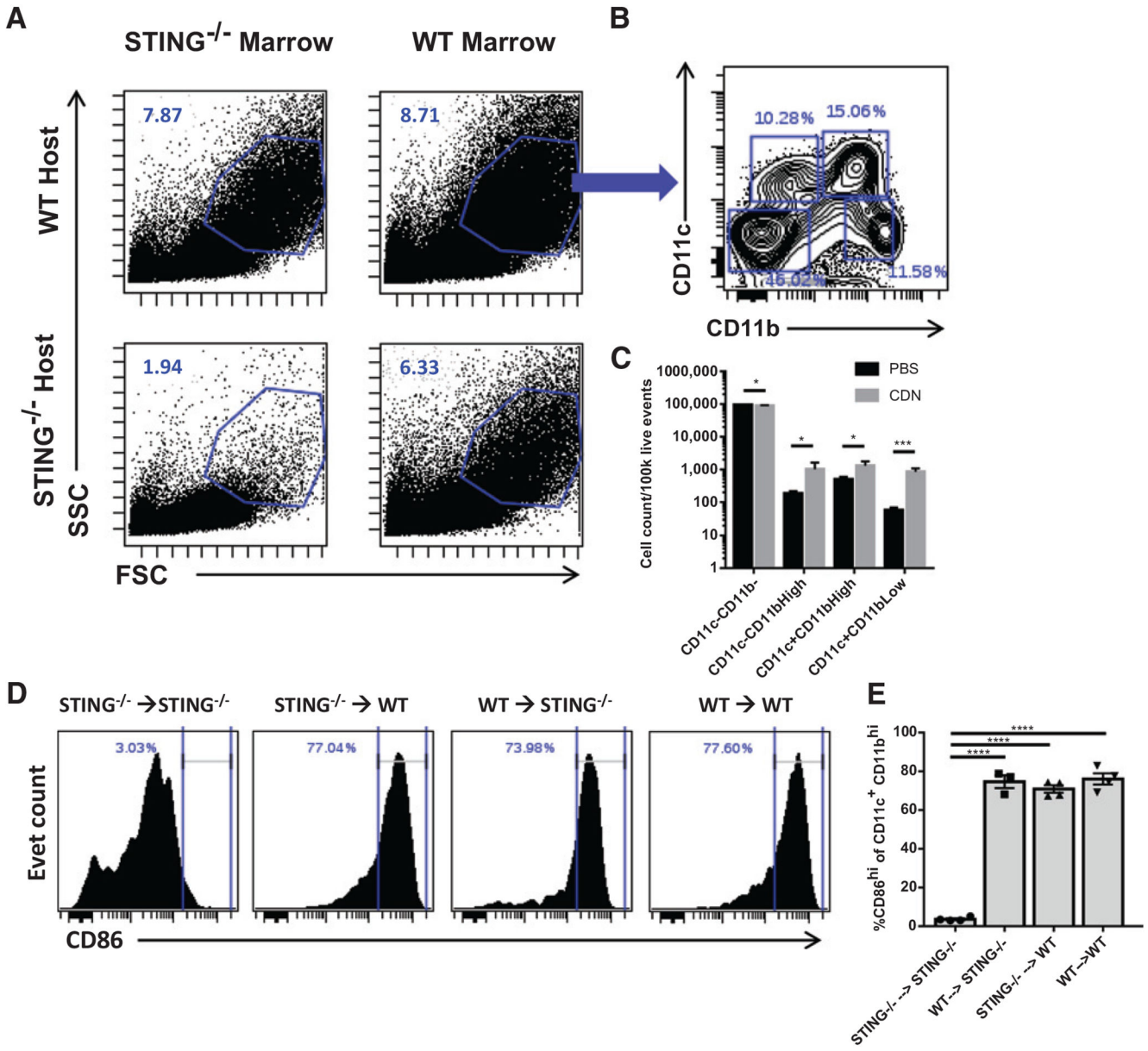

Figure 7.

APC activation can occur through multiple mechanisms. **A,** Gross characterization of theTDLNs in chimeric mice. Indicated STING chimeric animals were generated as in Fig. 6. B16F10 tumors were implanted, and animals were treated as in Fig. 1A. Inguinal TDLNs were analyzed 24 hours after i.t. CDN administration by flow cytometry. Plots are representative of two independent experiments with ≥3 biological replicates per experiment. **B,** Representative flow cytometry from WT→WT inguinal TDLNs. **C,** DC and monocyte/macrophage populations in the TME. Data from WT→WT TDLNs before and after i.t. CDN. *, $P < 0.05$ and ***, $P < 0.001$. **D,** APC activation in the TDLNs. Representative flow cytometry histograms of $FSC^{hi}SSC^{hi}$ $CD11b^{+}CD11c^{+}$ cells taken from each chimeric background and analyzed for CD86 surface expression after i.t. CDN administration. **E,**

Summary data from **D**. All error bars represent SEM. Plots are representative of two independent experiments with ≥3 biological replicates per experiment. ****, $P < 0.0001$.